Stability and Rendering Limitations of High-Performance Admittance Based Haptic Interfaces

Patrick Dills*, Kaitlyn Gabardi*, and Michael Zinn, *Member, IEEE*

***Abstract*— This work investigates the stability and rendering limitations of admittance-type haptic devices. We investigated a wider range of impedances than had previously been considered, including stiffness, damping, and mass and combinations thereof. The coupled human driving impedance, actuator position control bandwidth, and loop delay are identified as major factors affecting the range of stable impedances. Finally, the theoretical results are experimentally verified using a custom one degree of freedom admittance type haptic device.**

I. Introduction

Admittance-based kinesthetic haptic interfaces are well suited to render high forces and have been used in a wide range of applications. However, unlike impedance-based devices, the factors affecting the stable range of rendered impedances and the output impedance of admittance-controlled devices are not well understood. Early studies to define the range of achievable impedances in this sort of control approach were performed in the context of teleoperation and force control of industrial robots [1]. This early work studies the range of stiffness and damping that an admittance type device can achieve but does not consider a human interacting with the admittance-controlled robot. More recently, [2] studied the range of stable masses admittance controlled haptic devices can achieve when coupled to a human operator. Finally, passivity theory was applied in [3] to evaluate stability while a device is interacting with any passive driving point impedance but the analysis did not allow for the effects of time delays to be considered.

In the work presented here, we examine a wider range of impedances and identify factors including, position control bandwidth, delay, and the human's impedance which affect the stability and rendering performance of admittance control devices. The organization of this work is as follows: (1) a description of the modeling approach used in the analytical investigation, (2) an analytical investigation of factors effecting stability and rendering limits, (3) evaluation of output impedance as a function of system characteristics, (4) an experimental validation of the primary analytical results.

Research supported in part by a grant from the National Science Foundation (NSF Award No. 1830516)

*Patrick Dills and Kaitlyn Gabardi are co-first authors contributing equally to this work and are Graduate Students in the Department of Mechanical Engineering at the University of Wisconsin – Madison (gabardi|wisc.edu and pdills@wisc.edu)

Michael Zinn is an Associate Professor in the Department of Mechanical Engineering at the University of Wisconsin – Madison, (mzinn@wisc.edu)

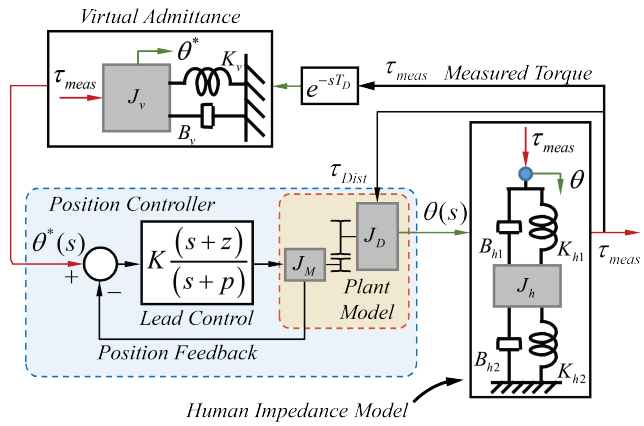

a) Conceptual diagram of an admittance controlled haptic device

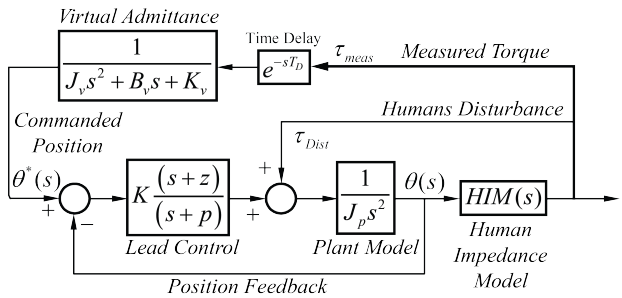

b) Block diagram of an admittance controlled haptic device

Fig. 1a) Conceptual dynamic system model of an admittance type haptic device and coupled human impedance position controller. b) Block diagram of the admittance controlled haptic device.

II. Approach to Stability Analysis

The dynamic model, conceptually shown in Fig. 1a and initially proposed in [2], can be used to analyze the asymptotic stability of an admittance based haptic device. The model includes a fast inner position control loop, typical of admittance-based controllers, utilizing a lead compensator, and an outer force control loop. In addition, time delay and human impedance coupling [4] are incorporated as they are likely to affect rendering stability [2]. The equivalent block diagram representation of the system dynamic model is shown in Fig. 1b.

Recognizing that high-performance admittance-based systems are commonly designed for high-dynamic stiffness, typically by incorporating a highly geared motor and a fast, high gain position controller, it is reasonable to ignore the effect that the reflected human interaction forces have on plant model inertia [5]. By doing so, the system model reduces to a single feedback loop where stability can be assessed by examining the open-loop transfer function (see Fig. 2).

© 2022 IEEE. Personal use of this material is permitted. Permission from IEEE must be obtained for all other uses, in any current or future media, including reprinting/republishing this material for advertising or promotional purposes, creating new collective works, for resale or redistribution to servers or lists, or reuse of any copyrighted component of this work in other works

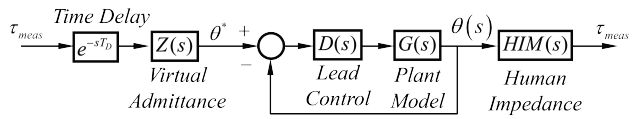

Fig. 2) Simplified open loop transfer function used to analyze stability of admittance devices.

III. Analytical Minimum Admittances and Combinations of Admittances

While admittance-based haptic interfaces can be used to render a wide variety of virtual admittances, typically mass-spring-damper terms are used in combination to express more complex rendering. As such, we will restrict our rendering stability analysis to these simple terms. Our analysis will first consider the stability of pure stiffness, damping, and mass terms. Then combinations of stiffness and damping, damping and mass, mass and stiffness are considered. Finally, we present a map of the full space with all combinations of mass stiffness and damping. In the subsequent analysis we will examine the effects of (1) position control bandwidth (2) delay and (3) the human's impedance on the stability of the admittance-based devices.

A. Factors Affecting the Minimum Stable Stiffness

The simplified model described in Fig. 2 can be used to analyze the minimum stable virtual stiffness where $Z(s) = 1/K_v$, where K_v is the virtual stiffness. We use the system parameters listed in Table 1 for the duration of the analytical section.

Table 1. Summary of Device and Human Impedance Parameters

Parameter's	K_{h1}	K_{h2}	B_{h1}	B_{h2}	J_h
Value	48.8	375	4.5	7.9	4.5
Units	[N/m]	[N/m]	[N/(m/sec)]	[N/(m/sec)]	[Kg]
Parameter's	Rotor Inertia J_m		Drive Inertia J_d		Ratio N
Value	$6.96\text{x}10^{-6}$		0.4181		260
Units	[Kg-m^2]		[Kg-m^2]		[Rad/m]

The frequency response of the simplified model's open-loop transfer function is shown in Fig. 3 along with the frequency response of the individual system components. By observing the phase contributions of each component of the system we see that a positive pure virtual stiffness will never be unstable without delay, as the system's net phase does not drop below -90 degrees in the absence of delay.

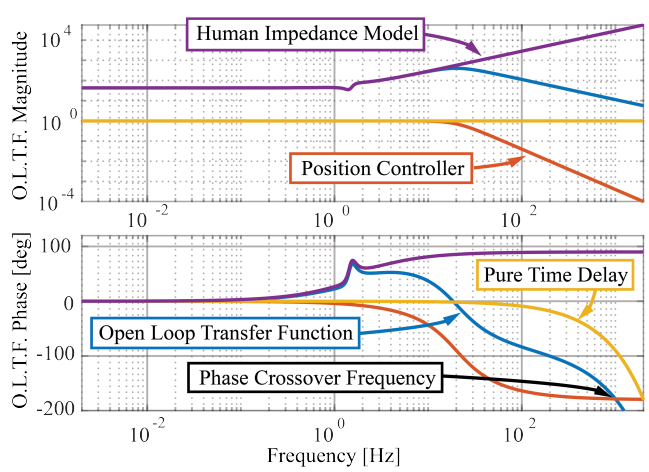

Fig. 3) Magnitude and phase contributions of each individual part of the simplified model and the full resulting open loop transfer function.

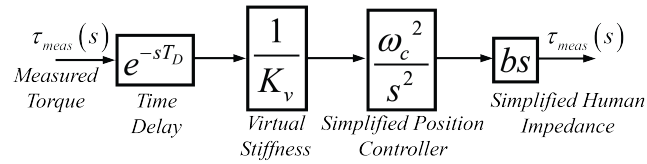

Fig. 4) High frequency simplification of the admittance control loops open loop transfer function while rendering a virtual stiffness.

Conversely, the system becomes unstable with the introduction of delay. Stability is determined by the properties of the system at the phase crossover frequency. For small time delays the phase crossover frequency will occur at a high frequency relative to the bandwidth of the position controller and human impedance model resonance. This leads to two high frequency model simplifications. First, the human impedance model can be simplified into a pure damper at high frequencies. Additionally, the position controller can be simplified at high frequencies by recognizing that the magnitude roll-off is connected to the system's natural frequency. A simplified block diagram of the system is shown in Fig. 4.

Examining the phase contributions of each of the components of the high frequency model shows that the phase crossover frequency will occur approximately at the frequency where the pure delay causes the net system to lose 90 degrees of phase. This results in the expression (1) for the phase crossover frequency of the simplified system.

$$\omega_{cross} = \frac{\pi}{2T_D} \tag{1}$$

Substituting (1) into the magnitude of the open loop transfer function (2), setting it equal to one, and solving for the virtual admittance leads to (3).

$$|OLTF| \approx \left| \frac{b\omega_n^2 e^{-sT_D} s}{K_v s^2} \right| = \frac{b\omega_n^2}{K_{v\,\frac{\pi}{2T_D}}} \tag{2}$$

$$K_{v\ \min} \approx \frac{b\omega_n^2 2T_D}{\pi} \tag{3}$$

Examination of this expression leads to three important results.

1. High frequency damping added by ***the human's impedance increases the minimum virtual stiffness***.
2. Increasing ***time delays can increase the minimum virtual stiffness***, if the phase crossover frequency is above the position control bandwidth.
3. ***Increasing the position control bandwidth will increase the minimum virtual stiffness***.

Interestingly, the relationship between an admittance-controlled device's minimum stable stiffness is opposite to results found pertaining to virtual mass in [2]. [2] showed increases in position control bandwidth decrease the minimum virtual mass.

It is also possible to find an expression showing the theoretical minimum virtual stiffness under infinite bandwidth conditions. Infinite bandwidth is of course impossible in reality. The expression represents a theoretical worst-case scenario in terms of bandwidth's effect on the minimum virtual stiffness. The crossover frequency can be

© 2022 IEEE. Personal use of this material is permitted. Permission from IEEE must be obtained for all other uses, in any current or future media, including reprinting/republishing this material for advertising or promotional purposes, creating new collective works, for resale or redistribution to servers or lists, or reuse of any copyrighted component of this work in other works

found by recognizing that the human impedance model adds 90 degrees of phase at high frequencies. Delay is the only term that subtracts phase from the system. Consequently, the systems phase crossover frequency occurs at the frequency where the pure delays phase equals -270 degrees or (4)

$$\omega_{cross} = \frac{3\pi}{2T_D} \tag{4}$$

Substituting the new phase crossover frequency into the magnitude expression (5) yields an expression showing the approximate minimum stiffness in the case of a very high bandwidth position controller (6).

$$|OLTF| \approx \left| \frac{bse^{-sT_D}}{K_v} \right| = \frac{b\frac{3\pi}{2T_D}}{K_v} \tag{5}$$

$$K_{v\ \min} \approx \frac{3\pi b}{2T_D} \tag{6}$$

Expression (6) indicates that ***delay can decrease the minimum stable stiffness*** if the devices phase crossover frequency is lower than the bandwidth of the position controller. While this is likely an uncommon situation for a pure stiffness it does highlight the possibility of this effect occurring. We will see in subsequent sections that when considering an admittance composed of mass stiffness and damping this effect becomes more plausible.

B. Factors Affecting the Minimum Stable Damping

We consider the delay free system with a pure damper as our virtual admittance. As in the case of virtual stiffness we find that the delay free system is stable for all positive virtual damping values as long as the position control bandwidth is sufficiently higher than the human resonance. This is true because the human's impedance adds 90 degrees of phase which is canceled out by the phase contribution of the pure virtual damper. As long as the position control bandwidth is higher than the human resonance the system's phase will asymptotically approach -180 degrees but will not cross -180 degrees, and thus the resulting gain margin is infinite.

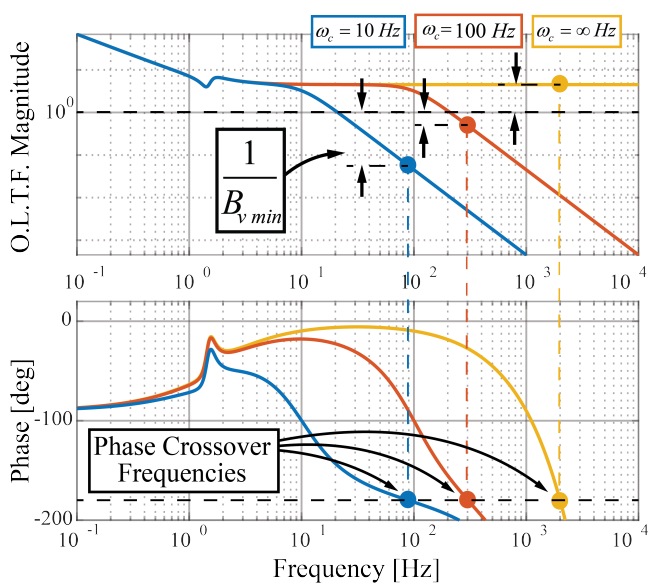

Fig. 5) Bode plots of the full system showing the effect of bandwidth on the minimum damping of the system.

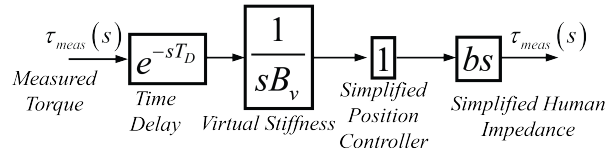

Fig. 6) Simplified open loop transfer function of the admittance control loop rendering a damper

Much like in the case of the pure virtual stiffness we must consider the simultaneous effect of position control bandwidth and delay on the stability of the time delayed system. However, the same high frequency position control approximation does not yield a closed-form approximation for the phase crossover frequency. However, it is easy to see from the system's bode plot, shown in Fig. 5, that increases in the position control bandwidth will increase the minimum virtual damping. This analysis shows that, just as in the case of virtual stiffness, ***the minimum stable damping is increased with an increase in position control bandwidth.***

Considering the high frequency gain of a pure damper with infinite bandwidth, see Fig. 5, shows the theoretical limit of the stability of the system as bandwidth increases. It's interesting to note that while we can solve for the phase crossover frequency in this case it does not affect the result. The theoretical stability limit can be derived from the magnitude expression of the simplified open loop transfer function (see Fig. 6) and is shown in (7) and (8).

$$|OLTF| \approx \left| \frac{bse^{-sT_D}}{C_v s} \right| = \frac{b}{C_v} \tag{7}$$

$$C_{v\ \min} \approx b \tag{8}$$

In the case of finite position control bandwidth, increasing time delays increases the minimum damping but this effect is limited. Even under large time delays the minimum damping will converge to the damping provided by the human operator. An examination of the magnitude of the system's frequency response shows a flat magnitude above the human resonance as well as below the position control bandwidth, contribute to this effect (see Fig. 5).

C. Factors Affecting the Minimum Stable Mass

The range of rendered mass that an admittance controlled haptic devices can achieve, when coupled to a human operator, can be identified with the methods presented in [2]. In short, the minimum mass is decreased with an increase in controller bandwidth. This is contrary to the results obtained in the two previous sections studying stiffness and damping where increases in bandwidth increased the minimum stable virtual stiffness and damping. Delay and the human's impedance also limit the minimum virtual mass, which is generally consistent with the results obtained in the previous sections on stiffness and damping.

D. Combinations of Stiffness and Damping

A similar analysis to the method presented in Section IIa and b. can be applied to combinations of stiffness and damping. The virtual impedance can re-written in bode form with a critical gain and is shown in Appendix A. One might think of this process as finding the critical gain or, alternatively, the minimum damping for a pole location defined by the ratio of virtual damping and stiffness.

© 2022 IEEE. Personal use of this material is permitted. Permission from IEEE must be obtained for all other uses, in any current or future media, including reprinting/republishing this material for advertising or promotional purposes, creating new collective works, for resale or redistribution to servers or lists, or reuse of any copyrighted component of this work in other works

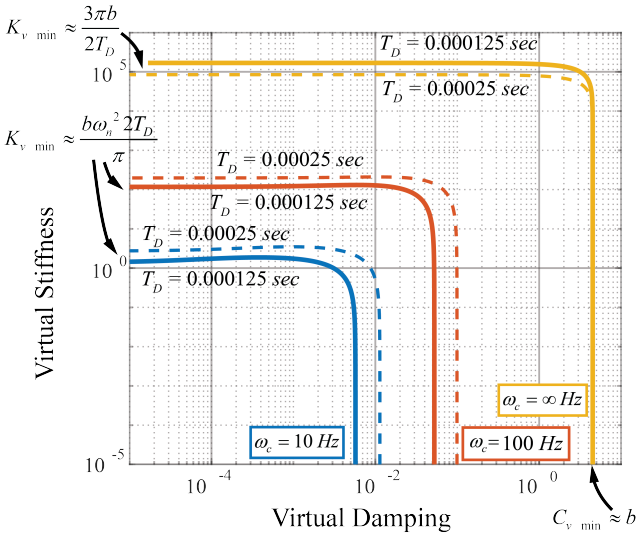

Fig. 7) Theoretical minimum stability curves for combinations of stiffness and damping over a wide range of position control bandwidths and at a constant delay. *Td* = 0.000125 [sec]. Dashed lines of the same color have the same position control bandwidth but have an increased delay time *Td* = 0.00025 [sec]

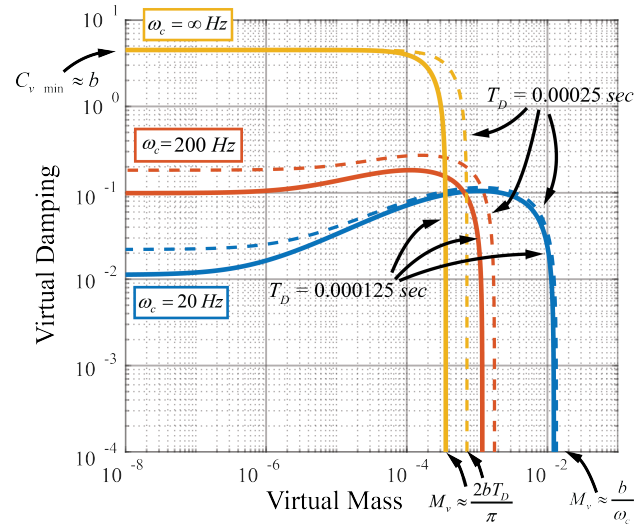

Fig. 8) Theoretical minimum stability curves for combinations of damping and mass over a range of position control bandwidths and at a constant delay. *Td* = 0.000125 [sec]. Dashed lines of the same color have the same position control bandwidth but have an increased delay time *Td* = 0.00025 [sec]

Numerically finding the phase crossover frequency for a range of given pole locations and identifying the critical gain allows us to evaluate the minimum virtual damping for a corresponding virtual stiffness. Varying the position control bandwidth under constant delay conditions yields the curves shown plotted in solid lines in Fig. 7. The effect of delay, plotted in dashed lines is also shown in Fig. 7.

A continuum of minimum stable stiffness and damping exists, as shown in Fig. 7 and trends shown in section IIa and IIb are also numerically confirmed on the axis of Fig. 7. In summary, increases in position control bandwidth and the human's high frequency damping uniformly increase the minimum stable combinations of stiffness and damping. Delay generally increases the minimum combinations of stiffness and damping. Although, in the infinite bandwidth case, impedances dominated by stiffness are reduced with an increase in delay.

E. Combinations of Damping and Mass

Combinations of damping and mass may be analyzed by recognizing that the virtual admittance can be rewritten in bode form as in Appendix B. Analyzing combinations of pure mass and damping results in curves shown in Fig. 8.

Similar to section II D, this process might be thought of as finding the minimum stable mass (critical gain) for a given pole location or corresponding damping value. Delay always has a negative effect for combinations of damping and mass and increases the critical gain. However, it is easy to see, from Fig. 8, that position control bandwidth has inverse effects on mass, and damping. Increases in position control bandwidth reduce the minimum mass until delay dominates the stability of the system. This is contrary to position control bandwidths effect on minimum damping where the minimum damping is increased with increases in position control bandwidth. The combination of these effects causes the minimum stable admittance curves to shift instead of uniformly shrinking and growing like in section IID.

F. Combinations of Mass, Stiffness and Damping

Combinations of mass stiffness and damping can be written in a normalized form as seen in (9). This is in fact the bode form for combinations of all three impedances.

$$Z(s) = \frac{1}{M_v s^2 + C_v s + K_v} = \frac{1}{K_v}\frac{\omega_n^2}{s^2 + 2\xi\omega_n + \omega_n^2} \tag{9}$$

By looping through the possible damping ratios and natural frequencies it is possible to map, see Fig. 9, the minimum stable combinations of virtual admittances (mass, springs and dampers). All of the features of the previous sections are represented in Fig. 9. When combining all three virtual admittances together, for a given natural frequency and damping ratio, achieving a smaller critical gain shrinks all three impedances simultaneously. Framing the analysis in this way allows us to evaluate the transparency directly.

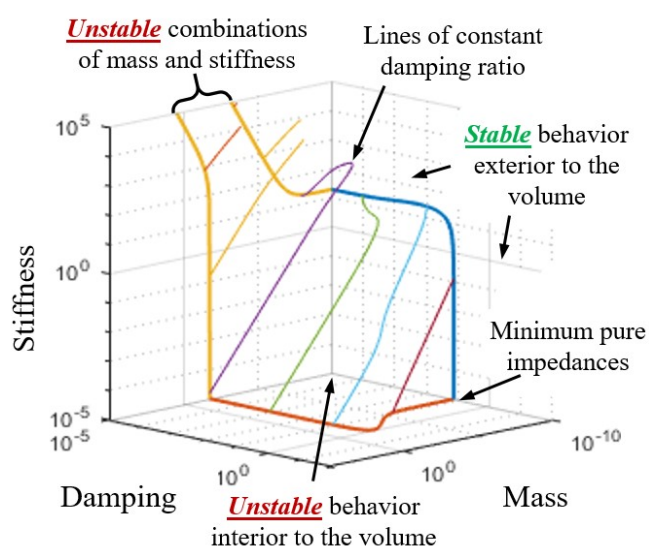

Fig. 9) Unstable combinations of mass stiffness and damping for an admittance device are interior to this volume. Pairs of impedances are Red: Damping and Mass, Blue: Stiffness and Mass, Yellow: Mass and Stiffness.

© 2022 IEEE. Personal use of this material is permitted. Permission from IEEE must be obtained for all other uses, in any current or future media, including reprinting/republishing this material for advertising or promotional purposes, creating new collective works, for resale or redistribution to servers or lists, or reuse of any copyrighted component of this work in other works

1) Position Control Bandwidth and Combinations of Mass Stiffness and Damping

Considering a system free of delay allows us to focus on the effect of position control bandwidth on the minimum complex impedance, as seen in Fig. 10. We approach this problem by first assuming a natural frequency and damping ratio for the normalized virtual admittance shown in (9).

As seen in Fig. 10, varying the position control bandwidth, for a fixed virtual admittance natural frequency, affects the loop gain at the phase crossover frequency which, in turn, determines if the overall admittance will increase or decrease with increased position control bandwidth.

If the position control bandwidth is less than the admittance resonant frequency the minimum gain increases with increases in position control bandwidth. This is similar to system behavior observed in the case of a pure virtual stiffness. Conversely if the position control bandwidth is greater than the virtual admittance resonant frequency the minimum virtual admittance decreases with increases in position control bandwidth which is analogous to stability behavior if rendering a pure inertia.

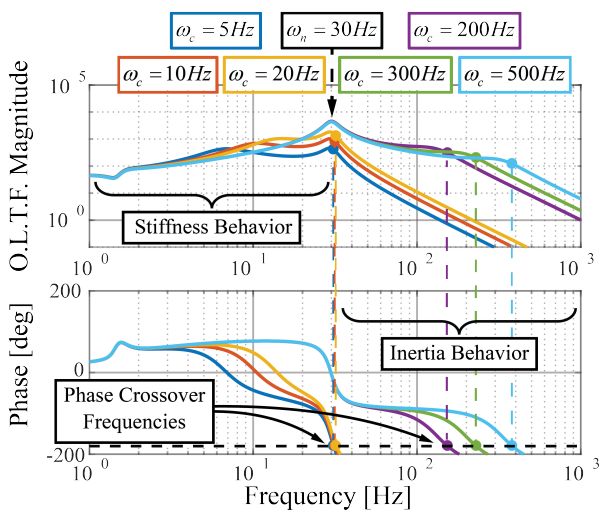

Fig. 10) The effect of position control bandwidth on a lightly damped virtual admittance composed of mass stiffness and damping.

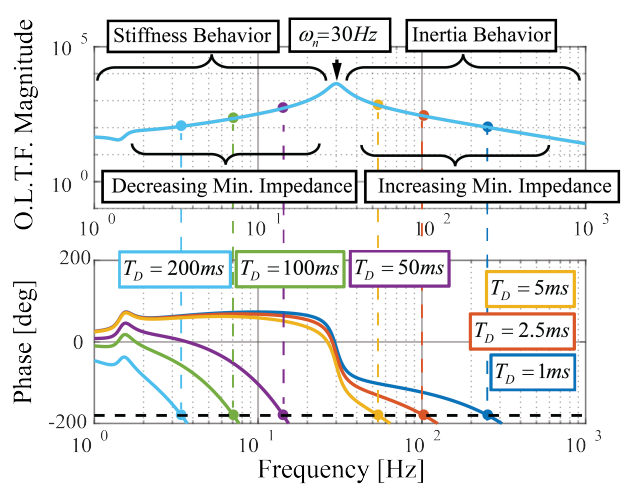

Fig. 11) Effect of delay on minimum stable gain while rendering combinations of mass stiffness and damping.

2) Time Delay and Mass Stiffness and Damping

Removing position control dynamics from the admittance control scheme's open loop transfer function, see Fig. 11, emphasizes effects of delay while rendering a complex impedance composed of mass stiffness and damping.

Delay uniformly decreases the phase crossover frequency leading to behavior as seen in infinite bandwidth stiffness virtual stiffness expression (6) and mass expressions [2].

The combined effects of effects of position control bandwidth and small delays generally yields similar results to the case of position control bandwidth alone (see Fig. 10). This is true because delay simply reduces the phase crossover frequency without affecting the magnitude of the open loop transfer function, resulting in lower phase crossover frequencies.

3) Lightly Damped Combinations of Admittances

Combinations of purely mass and stiffness have a unique behavior that other combinations of admittances don't display. As damping is eliminated from (9) ***a range of combinations of pure mass and stiffness exist where the system will never be asymptotically stable even for very large virtual admittances***.

Two critical frequencies define the boundaries of this completely unstable range of admittances. The first important frequency occurs approximately when the position control bandwidth is equal to the resonant frequency of the virtual admittance. At this frequency the system has infinite gain at the phase crossover frequency.

For an undamped admittance this behavior continues until a second critical frequency occurs. This frequency occurs when delay begins to dominate the phase crossover frequency (see Fig. 12), or where phase loss from delay cancels out the phase lead from the human's impedance. This is the same logic leading to (1). Ultimately, lightly damped systems do not have a completely unstable range of combinations of stiffness and damping but minimum admittances can still be quite large when the admittances natural frequency is in between these two critical frequencies.

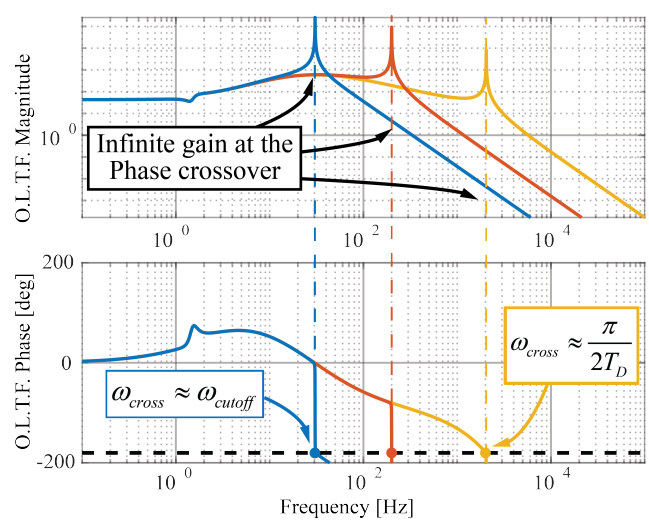

Fig. 12) Bode plots showing the system at two critical virtual admittance natural frequencies and an intermediary frequency.

© 2022 IEEE. Personal use of this material is permitted. Permission from IEEE must be obtained for all other uses, in any current or future media, including reprinting/republishing this material for advertising or promotional purposes, creating new collective works, for resale or redistribution to servers or lists, or reuse of any copyrighted component of this work in other works

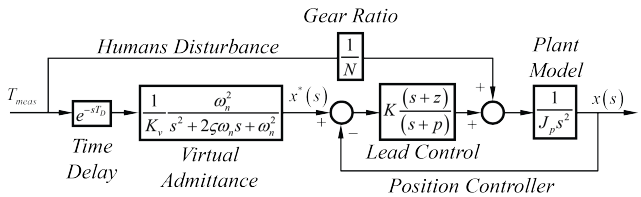

Fig. 13) Block diagram of the systems output impedance with time delay, a three parameter virtual admittance, the position controller and the humans disturbance explicitly modeled.

IV. Output Impedance of a Diverse Range of Virtual Admittances

Previously, [2] showed that relationships exist between the rendering bandwidth of virtual masses and both position control bandwidth and time delay. The rendering bandwidth was defined as the frequency where the phase of the systems output impedance reached 135 degrees. This definition works well when rendering pure masses, however it does not generalize to a wider range of impedances. Instead we choose to define the rendering bandwidth as the frequency where the systems output impedance differs from the desired impedance by 45 degrees of phase.

To utilize this definition, we first form the closed loop output impedance transfer function for our system (10) shown in block diagram form in Fig. 13.

$$\frac{F(s)}{V(s)} = \frac{G\left(e^{sT_D} + DNZ\right)}{e^{sT_D} N\left(DG+1\right)s} \tag{10}$$

A. Position Control Bandwidth and Rendering Range

Eliminating delay from (10) and plotting the systems impedance for a range of position control bandwidths, as seen in Fig. 14, shows that the system has a rendering bandwidth similar to [2]. The admittance control device has a rendering bandwidth which is directly proportional to the position control bandwidth.

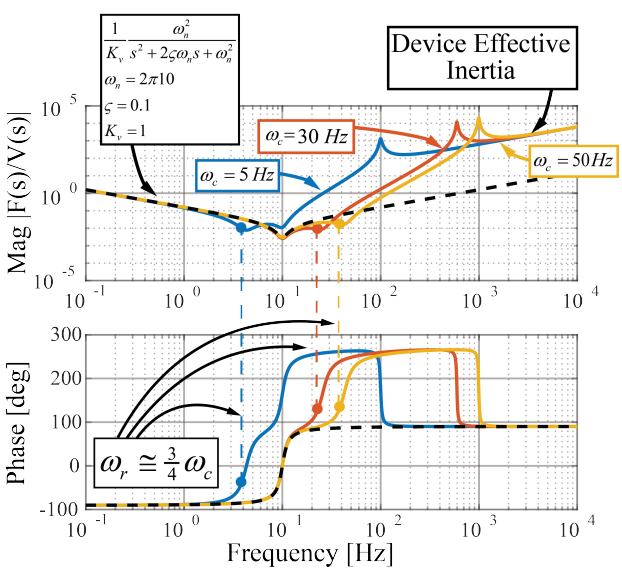

Fig. 14) The effect of position control bandwidth on the output impedance of an admittance controlled haptic device rendering a combination of mass stiffness and damping.

We find that the relationship from [2] and shown in (11) holds for combinations of mass springs and dampers with our altered definition of rendering bandwidth .

$$\omega_r \cong \tfrac{3}{4}\omega_c \tag{11}$$

Additionally, the systems impedance converges towards the open loop output impedance above the rendering bandwidth.

B. Delay and Rendering Range

Time delay also has the potential to affect an admittance controlled devices output impedance. Setting the position control bandwidth of the system to infinity results in a simplified impedance transfer function (12).

$$\frac{F(s)}{V(s)} = \frac{1}{e^{-sT_D} Zs} = K_v e^{sT_D} \frac{s^2 + 2\varsigma\omega_n s + \omega_n^2}{\omega_n^2 s} \tag{12}$$

At zero delay the devices output impedance simplifies to terms contributed by the virtual admittance. It follows that the rendering bandwidth is the frequency where delay adds 45 degrees of phase to the systems output impedance or (13).

$$\angle e^{j\omega_r T_D} = \frac{\pi}{4} \rightarrow \omega_r = \frac{\pi}{4T_D} \tag{13}$$

This is consistent with the results shown in [2] and would hold for any combination of impedances.

V. Experimental Stability Results

Stability results presented in sections II and III were validated using a custom one degree of freedom admittance type haptic device shown in Fig. 15. The human impedance model parameters were experimentally determined for a total of six participants, and the stable range of impedances were evaluated and compared to the theoretical stable regions as position control bandwidth and loop delay were varied.

A. Human Impedance Model Estimation

To verify each user's human impedance model parameters, a user was asked to grasp the input of the device and maintain a consistent grip as a range of sinusoidal frequencies between 1 and 30 Hz were commanded.

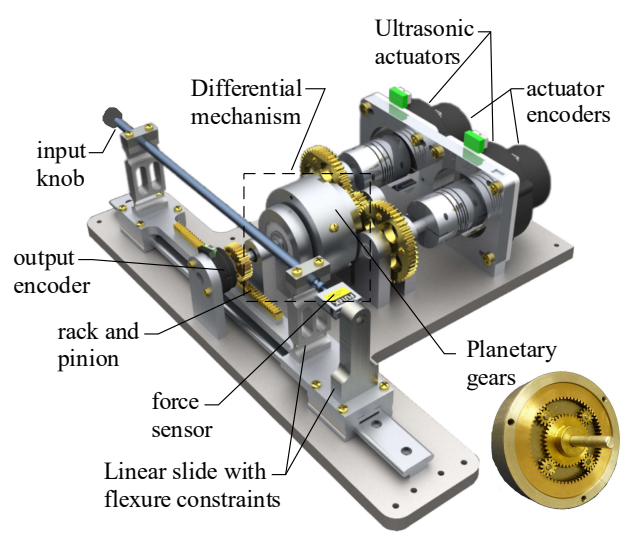

Fig. 15) Single degree of freedom admittance type haptic device used to test minimum mass stiffness and damping and combinations of admittances.

© 2022 IEEE. Personal use of this material is permitted. Permission from IEEE must be obtained for all other uses, in any current or future media, including reprinting/republishing this material for advertising or promotional purposes, creating new collective works, for resale or redistribution to servers or lists, or reuse of any copyrighted component of this work in other works

Device position device position and force were measured and the process was repeated for a total of three different grips: light, regular, and firm. The human impedance model parameters for each grip were determined by fitting a high-frequency approximation, and two-parameter model, used to represent the interaction force between the human arm and device during motion [4]. Throughout the experiments, participants were asked to maintain their regular grip and posture used during the human impedance model evaluation. A participant's range of human impedance model parameters were used to solve for the predicated stability curves and compare to the experimental regions of stability.

B. *Experimental Stiffness Evaluation*

The minimum damping and stiffness were evaluated for two different position control bandwidths (10 and 30 Hz) and delays (5 and 20 ms). To verify the minimum damping and stiffness, the rendered damping and stiffness were decreased until a user observed instability of the device in the form of unstable oscillations.

(3) showed that an increase in position control bandwidth and delay increases the minimum virtual stiffness. Fig. 16 compares analytical, numerical, and experimental results for the minimum stable virtual stiffness rendered by an admittance controlled haptic device. Error bars show the nominal measured humans' impedance along with the expected change in minimum virtual stiffness for a 20 percent change in the human's impedance. Fig. 16 confirms the minimum virtual stiffness expression, which shows that increasing position control bandwidth and adding small-time delays increase the minimum virtual stiffness. Additionally, the analytical solution matches numerical results quite closely.

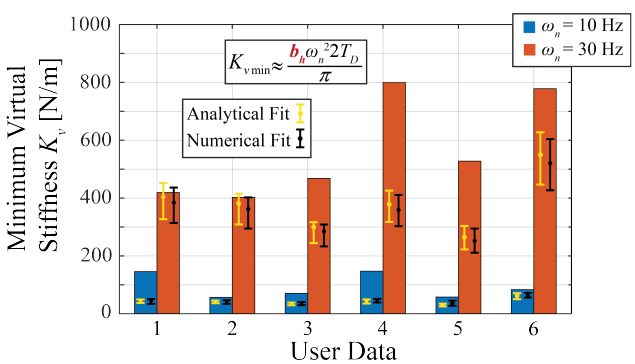

a) Varying bandwidth with a fixed delay

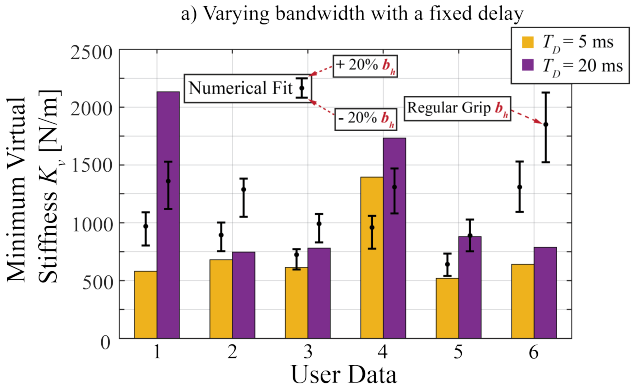

b) Varying delay with a fixed bandwidth

Fig. 16) Representative experimental minimum stiffness results along with predicted analytical and numerical minimum stiffness values.

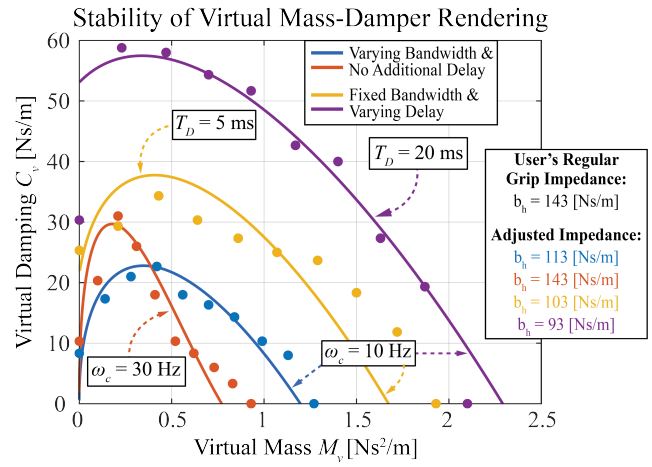

Fig. 17) Comparison between numerical and experimental minimum combinations of damping and mass for three different delays (blue yellow and purple, 0ms 5ms and 20ms respectively) and two different bandwidths (10hz – blue yellow and purple) (30Hz – red).

A. *Mass and Damping Stability Validation*

To evaluate the stable range of mass and damping, we first determined the minimum pure mass using the same approach as damping and stiffness. For a given mass, virtual damping was decreased until unstable oscillations were observed.

Measuring and fitting a linear model to a human's impedance is difficult and variations in a person's grip, posture, and limb co-contraction can impact their output impedance. We qualitatively observed these variations throughout the duration of the user study. Often a user becomes more skilled at interacting with the device over the course of running stability tests. We surmise that users varied and adapted their grip and impedance throughout the study despite being instructed to maintain a grip consistent with their nominal grip measured at the beginning of the user study. To accommodate this variation, we have used an adjusted human impedance value to fit theoretical curves to experimental user results shown in Fig. 17. The user data and stability boundaries shown in Fig. 17 are representative of the stability tests for all six subjects. Only small variations from the measured nominal grip human impedance are necessary to achieve the theoretical curves shown in Fig. 17. The adjusted damping values are tabulated in relation to the nominal measured value in Fig. 17 as well.

Experimental mass-damper stability regions align with results presented in section IIe. Fig. 17 shows that an increase in position control bandwidth has inverse effects on damping and mass resulting translations of the blue and red curves. Delay uniformly increases the minimum gain and the region of unstable behavior increases for combination of mass and damping.

A. *Mass, Damping, and Stiffness Stability Validation*

Utilizing the virtual admittance equation (9), a fixed natural frequency (ω_n = 30 Hz) was used for the combined mass spring and damper virtual admittance. For a given damping ratio, the minimum stiffness was decreased until a participant observed unstable oscillations.

© 2022 IEEE. Personal use of this material is permitted. Permission from IEEE must be obtained for all other uses, in any current or future media, including reprinting/republishing this material for advertising or promotional purposes, creating new collective works, for resale or redistribution to servers or lists, or reuse of any copyrighted component of this work in other works

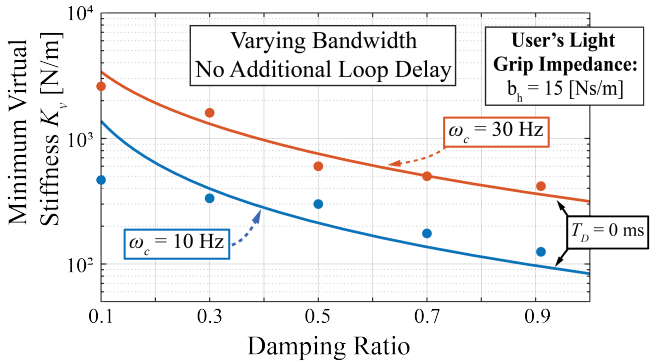

a) Varying bandwidth with a fixed delay

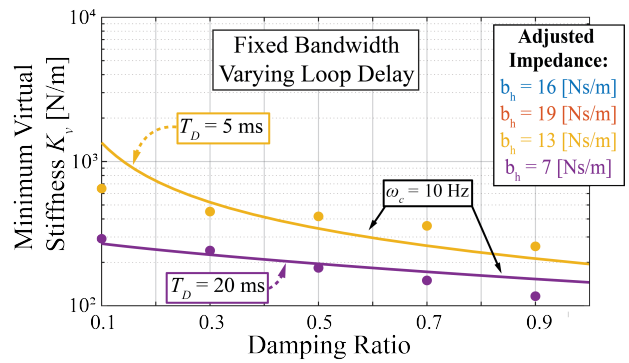

b) Varying delay with a fixed bandwidth

Fig. 18) Stability curves while rendering mass stiffness and damping simultaneously a) varies bandwidth with a fixed delay b) Varies delay under fixed bandwidth conditions.

We find that stability results from the theoretical model adjusted approximately for a user's light grip fits the experimental data well. Again, data shown in Fig. 18 is representative of a good fit from the six users tested. With no additional loop delay, Fig. 18 shows an increase in position controller bandwidth causes the region of stability to decrease, or the minimum virtual stiffness to increase for a given damping ratio. In contrast, when adding additional loop delay, an increase in delay increased the region of stability.

VI. Conclusion

This work examined the stability of admittance controlled haptic devices under a wider range of admittances than in prior work. The effect of the human impedance was directly considered and factors such as the systems position control bandwidth and internal delay were shown to have unique stabilizing or destabilizing effects on the control loop as a whole.

Future work includes expanding on factors that affect the model presented in this work. Compliance and inertia on the output of the device change the stability properties of the system and distort the systems output impedance. Further study could formalize the effects of device inertia and compliance on the stability and output impedance of admittance type haptic devices.

Appendix

A. Combinations of Stiffness and Damping

Putting a virtual admittance of combinations of stiffness and damping in bode form (14) shows that for a given pole location and open loop transfer function there is a critical damping value. This critical damping value also defines a corresponding stiffness for each minimum damping value.

$$Z(s) = \frac{1}{C_v s + K_v} = \frac{1}{C_v}\frac{1}{\left(s + \frac{K_v}{C_v}\right)} = K_{crit}\frac{1}{(s+p)} \tag{14}$$

The procedure for drawing the boundary between stable and unstable combinations of mass and damping then becomes a matter of assuming a pole location identifying the critical gain at the phase crossover frequency and back calculating minimum combinations of mass and damping.

B. Combinations of Damping and Mass

Putting a virtual admittance composed of combinations of Mass and damping in bode form (15) shows that for a given pole location there is a critical mass value. This critical mass also defines a corresponding damping for each minimum mass. Drawing the stability boundary for combinations of mass and damping follows the same procedure as in appendix A.

$$Z(s) = \frac{1}{M_v s^2 + C_v s} = \frac{1}{M_v}\frac{1}{s\left(s + \frac{C_v}{M_v}\right)} = K_{crit}\frac{1}{s(s+p)} \tag{15}$$

Acknowledgment

This work was made possible in part with the support of NSF Award No. 1830516

References

[1] D. Lawrence and R. Stoughton, "Position-based impedance control - Achieving stability in practice," presented at the Guidance, Navigation and Control Conference, Monterey,CA,U.S.A., Aug. 1987. doi: 10.2514/6.1987-2265.

[2] C. Parthiban and M. Zinn, "Performance and stability limitations of admittance-based haptic interfaces," in *2018 IEEE Haptics Symposium (HAPTICS)*, San Francisco, CA, Mar. 2018, pp. 58–65. doi: 10.1109/HAPTICS.2018.8357153.

[3] A. Q. Keemink, H. van der Kooij, and A. H. Stienen, "Admittance control for physical human–robot interaction," *Int. J. Robot. Res.*, vol. 37, no. 11, pp. 1421–1444, Sep. 2018, doi: 10.1177/0278364918768950.

[4] J. E. Speich, L. Shao, and M. Goldfarb, "Modeling the human hand as it interacts with a telemanipulation system," *Mechatronics*, vol. 15, no. 9, pp. 1127–1142, Nov. 2005, doi: 10.1016/j.mechatronics.2005.06.001.

[5] C. Parthiban and M. R. Zinn, "A simplified approach to admittance-type haptic device impedance evaluation," in *2014 IEEE Haptics Symposium (HAPTICS)*, Houston, TX, USA, Feb. 2014, pp. 587–590. doi: 10.1109/HAPTICS.2014.6775521.

© 2022 IEEE. Personal use of this material is permitted. Permission from IEEE must be obtained for all other uses, in any current or future media, including reprinting/republishing this material for advertising or promotional purposes, creating new collective works, for resale or redistribution to servers or lists, or reuse of any copyrighted component of this work in other works